Chapter 2
Dynamic and Cyclic Properties of Soils

2.1 Introduction

Response of soil depends on both the mechanical properties of soil itself and the nature of loading. Many geotechnical engineering problems are associated with dynamic and cyclic loadings, such as ocean wave or ice loading applied on foundations of offshore structures or bridges, dynamic loading applied on foundations of offshore wind power structures, ocean wave loading on harbor structures, seismic wave propagation through soils, machine vibration-induced loading on foundations, seismic loading, liquefaction and cyclic transient loading, and dynamic working loads [113].

Soils' responses subject to dynamic and cyclic loadings are strongly controlled by the mechanical properties of the soil, which basically include shear modulus (shear wave velocity), damping, Poisson's ratio, and density (mass). Of these, shear modulus and damping are the most important material properties with which to characterize the dynamic behavior of soils. Both these properties are affected by effective stress and over-consolidation ratio. While the determination of shear modulus is normally well established, the damping modeling is less clearly understood. Furthermore, both shear modulus and damping depend on the strain level, while the strain response level also depends on the modulus and damping. Moreover, at high strain levels, in addition to the strain level, other parameters such as rate and number of cycles of cyclic loading are also important influences on the shear modulus. The strain rate of soils due to dynamic loading also influences soils' strength (mainly for clay soils) and shear modulus, as will be presented in Sect. 2.5. Volume change characteristics are also important at high strain levels. In addition, the location of the water table, degree of saturation, and grain size distribution may be important, especially when liquefaction is a potential problem. All the issues above complicate the geotechnical analysis and challenge analysis accuracy requirements.

J. Jia, *Soil Dynamics and Foundation Modeling*,
https://doi.org/10.1007/978-3-319-40358-8_2

The constitutive relationship of soils can normally be categorized into two classes: At extremely small strain levels of soils, perfectly elastic (fully recoverable) behavior can be assumed; as the strain amplitude increases, the soil stiffness decreases and the plastic soil behavior has to be accounted for. This information will be presented in Sect. 2.3.

Experimental observations also show that the stiffness observed for a subsequent stress path depends on the immediate past history of soils. Stress paths that represent a continuation of the immediate past stress path result in the lowest stiffness, while those involving a complete reversal of direction result in the highest stiffness. Intermediate values are observed for stress paths that represent a sudden change of direction from the immediate past history [117].

Various types of constitutive equations are proposed to describe the stress–strain–strength behavior of materials. However, in most of the conventional design methods, simpler representations of material behavior are typically assumed. An example of such conventional design methods is a bearing capacity analysis (Chap. 12), which assumes a rigid perfectly plastic behavior of soils. On the other hand, separate deformation calculations often assume linear-elastic behavior.

Under static loads, such as gravity loads, the material behavior of soil for both clay and sand can normally be considered as linear-elastic. Under cyclic loadings, meanwhile, such as earthquake loading or ocean storm wave-induced loading, the cyclic soil behavior is more complex than for its static counterpart. The cyclic behavior of soils is responsible for many geotechnical failures, such as slope instability due to degradations in soils' properties subject to earthquake loading. The stress–strain response is then considered elastic-plastic, and even the strength is nonlinear and depends on the strain, stress, and possibly strain rate.

For clay, plasticity may be formulated based on the multi-surface (nested surfaces) concept, with an associated flow rule. The yield surfaces are normally of von-Mises type as shown in the left figure of Fig. 2.1. For sand, plasticity can also be formulated based on the multi-surface concept, but with a non-associative flow rule [123] to reproduce dilatancy effect, and the yield surfaces can be modeled as Drucker-Prager type shown in the right figure of Fig. 2.1.

Hardin and Drnevich [115] discussed the relative importance of parameters affecting shear modulus and damping. Shear strain amplitude, effective stress level, and void ratio were listed as affecting shear modulus mostly in clean sands. Damping was considered to be affected by these too, with the number of loading cycles also being a major influencing factor. For clays, the increase in the number of loading cycles has been correlated to a decrease in shear modulus with associated pore pressure increase, as summarized by Idriss and his co-workers [116]. Over-consolidation ratio (OCR) and plasticity index (I_p) also influence the clay behavior.

As discussed in Sect. 1.10, to perform a site-response analysis, if the shear strain under seismic or other types of cyclic loading is less than 10^{-6}, a linear soil model by modeling the soil with an initial shear modulus is preferred due to both its wide availability and computational convenience. In case the shear strain γ is in the range

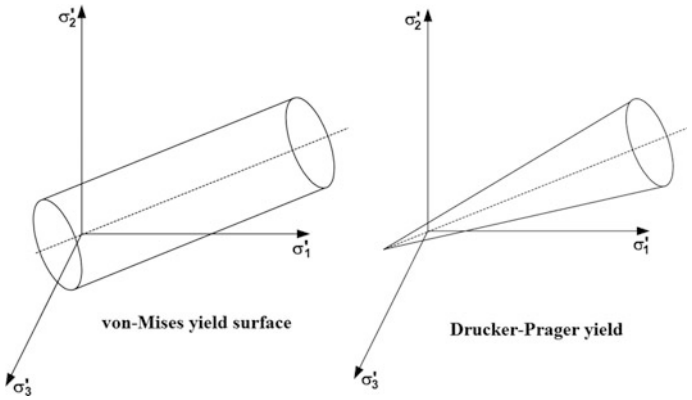

Fig. 2.1 von-Mises (left) and Drucker-Prager (right) yield criteria in principal stress space (σ_1', σ_2', and σ_3' are the maximum, intermediate, and minimum principal stresses)

$10^{-6} \leq \gamma \leq 10^{-2}$, in most cases the site response due to seismic loading is evaluated using the equivalent linear method (as will be presented in Sect. 2.2), in which compatible values of shear modulus and damping ratio are chosen according to the shear strain level in soil deposit. However, in this simplified method, the developed pore-water pressure and the residual soil displacements cannot be calculated, even though the ground motion response can be related to the liquefaction potential through approximation (Chap. 7). If shear stain responses are very large (above 10^{-2}) and/or there is permanent strain (the shear strain is not zero when the shear stress is zero), the soil actually exhibits elasto-plastic behavior, and it is recommended to use cyclic nonlinear modeling of soils (Sect. 2.4), which can model the actual stress–strain path and soil's stiffness degradation. In this more complicated soil modeling, the developed pore-water pressure and the residual soil displacements can be calculated by cyclic nonlinear soil models.

In the determination of soil properties, engineers should always bear in mind that the selected soil properties must produce safe design results. If a design is sensitive to variations in the soil properties being considered, a sensitivity analysis should be performed (Sect. 1.14).

Chen [114] provided three criteria for evaluating soil modeling. The first is a theoretical evaluation of the models with respect to the basic principles of continuum mechanics to ascertain their consistency with the theoretical requirements of continuity, stability, and uniqueness. The second criterion is to perform evaluation of the models with respect to their suitability to fit the laboratory test data from available test results and the ease of the determination of the material parameters from standard test data. The third one is to perform numerical evaluation of the models with respect to the implementation convenience of the modeling into computer calculations.

In summary, mainly depending on the amplitude of dynamic loading, the soil characteristics, and the resultant soil response, soils can generally be modeled by

three classes of models: equivalent linear models (Sects. 2.2 and 2.3), cyclic nonlinear models (Sect. 2.4.2), and more dedicated advanced constitutive nonlinear models (Sect. 2.4.4). Of these, the equivalent linear models require the description of the degradation of soil's secant shear modulus and damping with the change of shear strain, whereas the cyclic nonlinear models use backbone curves together with a number of rules that govern the unloading and reloading behavior and other effects, and the advanced constitutive soil models describe the soil's mechanical properties using constitutive laws, which is capable of reproducing a more realistic nonlinear response. Due to the simplicity of equivalent linear models, they are most widely used in site-response analysis, as will be presented in Chap. 3. They work fairly well at low strain levels, which are normally associated with mild seismic motions. At high shear levels, nonlinear models (Sect. 2.4) are usually adopted.

2.2 Equivalent Linear Soil Models

2.2.1 Equivalent Shear Modulus Modeling

For soils a certain level below the ground surface and far from adjacent structures, under symmetric cyclic loadings, the shear stress–strain relationship exhibits a hysteresis loop, as shown in Figs. 2.2 and 2.15. The hysteresis loop of a typical soil can be described by the path of the loop itself or by parameters that describe its shape. These parameters are the inclination and the breadth of the hysteresis loop, shear modulus, and damping.

Figure 2.3 shows a hysteresis loop describing variations of secant stiffness with the number increase in cyclic loading, which is used to describe the secant stiffness degradation of soils in an equivalent linear model shown in Fig. 2.5. In Fig. 2.3, it can be seen that the openness of the hysteresis loop increases with strain amplitude, which is actually an effect of the immediate past history of the soil.

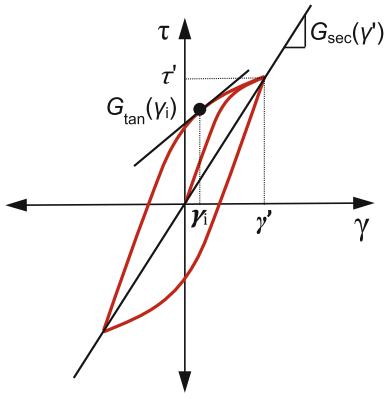

Fig. 2.2 Secant shear modulus G_{sec} and tangent shear modulus G_{tan} in a hysteresis loop (τ' and γ' are shear stress and shear strain, respectively)

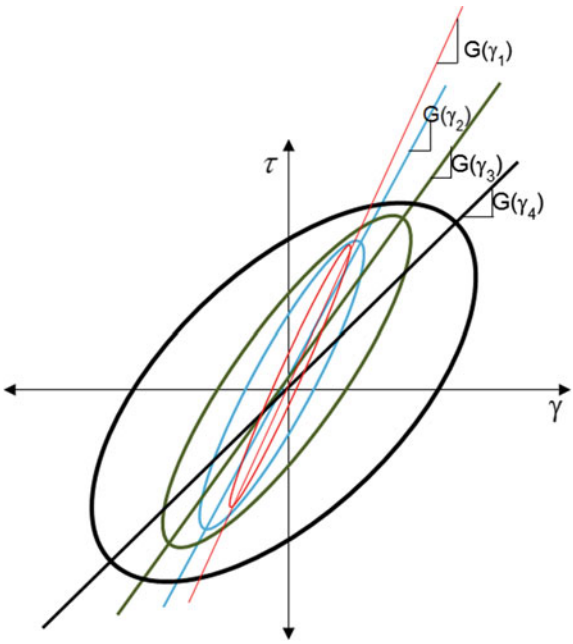

Fig. 2.3 Variation of the secant shear modulus with the number increase (1, 2, 3 …) of cyclic loading in an equivalent linear model

Furthermore, the tangent shear modulus $G_{\tan}$ (Fig. 2.2) changes along the path of the hysteresis loop under cyclic loadings. At low shear strain amplitudes, the tangent shear modulus is high and vice versa. However, one may approximate the average value of the tangent shear modulus over the entire loop as the secant shear modulus $G_{\sec}$:

$$G_{\sec} = \frac{\tau'}{\gamma'} \tag{2.1}$$

Note that the secant shear stiffness is strongly influenced by the shear strain amplitude, i.e., it decreases with an increase in shear strain. The locus of points corresponding to the tips of hysteresis loops of cyclic strain amplitudes forms a backbone shape shown in Fig. 2.4. From this figure, it is obvious that at zero strain, the shear modulus reaches its maximum value $G_{\max}$. In an equivalent linear model, the modulus ratio $G_{\sec}/G_{\max}$ (often written as $G/G_{\max}$) is usually adopted to describe the secant shear stiffness degradation of soils, resulting in a modulus reduction (also called normalized shear modulus) curve as shown in Fig. 2.5, which describes the same information as the backbone curve (Fig. 2.4). Furthermore, they can be determined from each other. The shear modulus reduction curves for coarse- and fine-grained soils are commonly modeled separately. However, the backbone curve cannot reflect a gradual transition of the modulus reduction curve between non-plastic coarse-grained soil and plastic fine-grained soils [1].

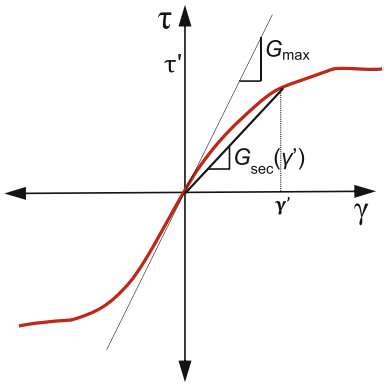

Fig. 2.4 Modulus reduction curve represented by a backbone curve showing the secant shear modulus, G_{sec}, and maximum shear modulus G_{max}

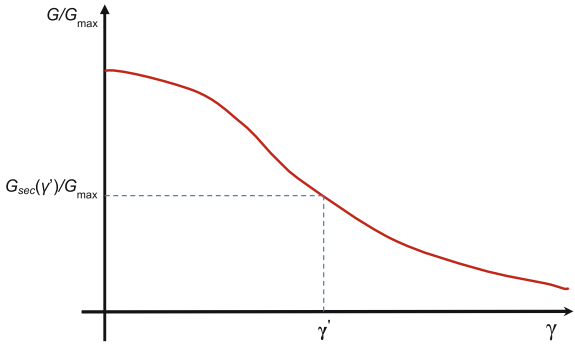

Fig. 2.5 Normalized shear modulus reduction curve

Figure 2.6 shows widely used modulus reduction curves proposed by Vucetic [118]. The charts are recommended only for preliminary studies due to large data scatters [231].

It is important to point out that the nonlinear curves shown in Figs. 2.4, 2.5, and 2.6 are essentially hypoelastic models because unloading occurs along the loading path. Under cyclic loading, these models do not account for hysteretic behavior as shown in Fig. 2.2 and possible residual displacements as observed for real soils, which can be implemented by nonlinear soil modeling (Sect. 2.4).

The soil stiffness is affected by many parameters such as the soil type, cyclic shear strain level, plasticity index, mean effective confining stress (more significant for soils with low plasticity), loading history, frequency of loading, number of loading cycles, over-consolidation ratio, void ratio, degree of saturation, grain characteristics. For example, the soil stiffness is significantly influenced by soil plasticity, i.e., the stiffness of soils with high plasticity decreases more slowly with the increase in shear strain than that of the low-plasticity soils.

Tests are needed to characterize dynamic soil properties, mainly including soils' shear wave velocity and damping. Generally, the test methods can be categorized as direct field measurement (such as seismic reflection test, seismic refraction test,

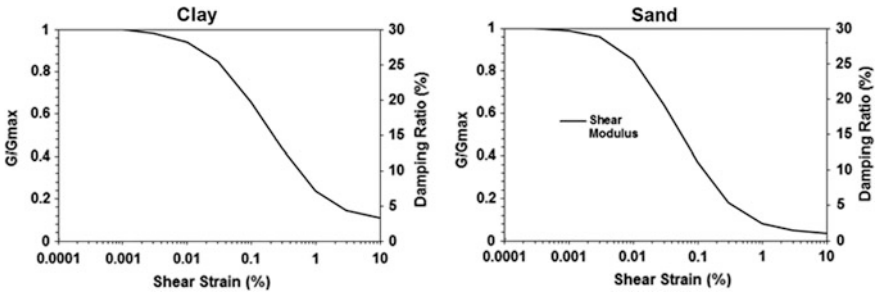

Fig. 2.6 Typical normalized shear modulus reduction curves for clay (left) and sand (right)

seismic cross-hole test, seismic down-hole test, up-hole test, suspension logger test), indirect field measurement (such as a correlation with standard penetration blow-count as discussed in Sect. 1.9.5), and laboratory measurement (such as resonant column test or bender elements test). The test can also be categorized as either measuring the local strain in triaxial testing using linear variable differential transformer (LVDT) [121] and submersible proximity sensor [122], or laboratory testing under quasi-static loading, including the use of dynamic testing, such as resonant column, bender elements, and cyclic triaxial testing. They are valid at different levels of shear strain, as shown in Fig. 2.13.

All tests that characterize soil behavior need to apply the initial stress conditions and anticipate cyclic loading as best as possible. The geophysical field tests have the advantage of testing undisturbed soil in actual field conditions, with the effective stress and drainage conditions that pertain in practice, while the laboratory tests need to confine and consolidate the soil sample back to the state of stress to replicate field conditions. Therefore, G_{max} obtained from the laboratory test is normally lower than that in the field due to the sample disturbance or limited reconsolidation time in the laboratory. For more details about those methods, readers may read Chap. 6 and sources [1] and [194].

In summary, through extensive research on dynamic soil properties, it may be generally concluded that, for sands, shear strain amplitude, effective stress level, and void ratio are the most dominant parameters affecting shear modulus and soil damping [115]. For clays, an increase in the number of loading cycles has also been correlated to a decrease in shear modulus with associated pore pressure increase, as summarized by Idriss et al. [116]. In addition, the over-consolidation ratio (OCR) and plasticity index (I_p) are also rather influential parameters to affect clay behavior. For various proposed shear modulus reduction curves used for equivalent linear soil models, see Sect. 2.3.2.

Moreover, as discussed in Sect. 2.5, it is widely recognized that shear modulus can also be significantly influenced by a variation in strain rate. G_{max} increases with the increase of strain rate. The effects of strain rate on shear modulus will increase with an increase in soil plasticity. Nevertheless, when using equivalent linear soil

models, it is generally acceptable to neglect the dependency of soil properties due to strain rate.

Readers may be reminded that, if it is necessary to calculate motion time histories among various depths of the soil, nonlinear time domain analysis is preferred to the equivalent linear analysis in frequency domain, because the nonlinearity of the springs, and more importantly the phase of motions at different soil depths, can be explicitly accounted for. As an example, at different depths, kinematic loading on pile foundations can vary to a certain extent, as will be discussed in Sects. 19.2.2 and 3.5.2.

For more details on the calculation of the shear stiffness, source [1] is recommended.

2.2.2 *Determination of* $G_{\max}$

Given that the shear strain is smaller than $3 \times 10^{-4}\%$, the maximum shear modulus $G_{\max}$ can be calculated directly by measuring soils' shear wave velocity v_s:

$$G_{\max} = \rho v_s^2 \tag{2.2}$$

Most soils such as loose gravel and sand have a shear wave velocity ranging from 330 to 1200 m/s. If soils are firm gravel or soft rock, the shear wave velocity increases to within the range 1200–2300 m/s. For stiff gravel and hard rock, this value further increases to the range 2300–6600 m/s. To give a feeling for the rate of shear velocity, the velocity of sound is 330 m/s in air and around 1500 m/s in water. Table 2.1 shows typical ranges of shear wave velocities for various types of soils.

In many cases, as the measured shear wave velocity is not available, the $G_{\max}$ can be assessed by correlating it with other soil properties such as the void ratio (e), over-consolidation ratio (OCR).

Table 2.1 Typical ranges of shear wave velocities for various types of soils [119]

Soil type	Shear wave velocity (m/s)
Dry silt, sand, loose gravel, loam, loose rock, moist fine-grained top soil	180–750
Compact till, gravel below water table, compact clayed gravel, cemented sand, sandy clay	750–2250
Weathered rock, partly decomposed rock, fractured rock	600–3000
Sound shale	750–3300
Sound sandstone	1500–4200
Sound limestone and chalk	1800–6000
Sound igneous rock (granite, diabase)	3600–6000
Sound metamorphic	3000–4800

Section 1.11.2 presents the relative increment $\left(\frac{G_{max}}{G_0}\right)$ of the maximum dynamic shear modulus due to soil consolidation.

The shear wave velocity v_s is a linear function of void ratio (e) and depends on the mean effective normal stress p' with a power of $n/2$, as proposed by Hardin and Richart [120]:

$$v_s = C(B - e)p'^{n/2} \tag{2.3}$$

where B, C, and n are constants depending on the type of soils.

The total mass density of soil ρ is a function of soil particle density ρ_s and the void ratio e:

$$\rho = \rho_s/(1 + e) \tag{2.4}$$

By combining the three equations above, one obtains:

$$G_{max} = \rho_s C^2 (B - e)^2 p'^n/(1 + e) \tag{2.5}$$

From laboratory tests, it is suggested that the maximum shear modulus may be calculated as:

$$G_{max} = 625 \cdot F(e) \cdot (\mathrm{OCR})^k \cdot p_a^{1-n} \cdot (\sigma'_m)^n \tag{2.6}$$

where $F(e)$ is a function of void ratio e, and it may be taken as $1/(0.3 + 0.7e^2)$ [147] or $1/e^{1/3}$ [148]; σ'_m is the mean principal effective stress; k is an over-consolidation ratio exponent related to plasticity index (I_p) as shown in Table 2.2; p_a = 100 kPa is the atmosphere pressure with the same unit as σ'_m and G_{max}; n is the stress component and is usually taken as 0.5, but can be computed for individual soils at different effective confining pressures [1].

By adopting $F(e) = 1/(0.3 + 0.7e^2)$ proposed by Hardin in 1978 [147] and assuming that the soil is normally consolidated (OCR = 1), the equation above can be rewritten as:

$$G_{max} = 625 \cdot \left(p_a \cdot \sigma'_m\right)^{0.5} / \left(0.3 + 0.7e^2\right) \tag{2.7}$$

Based on the effective octahedral stress σ'_{oct} and the void ratio e, Harding and Drnevich [141] also proposed another maximum shear modulus calculation in 1972:

$$G_{max} = 3230 \cdot \left(\sigma'_{oct}\right)^{0.5} (2.793 - e)^2/(1 + e) \tag{2.8}$$

Earlier, in 1970, Seed and Idriss [149] proposed a calculation of maximum shear modulus:

Table 2.2 Over-consolidation ratio exponent k varied with I_p [141]

I_p (%)	k
0	0.00
20	0.18
40	0.30
60	0.41
80	0.48
≥ 100	0.50

$$G_{max} = 22 \cdot K_{2,max} \cdot \left(p_a \cdot \sigma'_m\right)^{0.5} \tag{2.9}$$

where $K_{2,max}$ is determined by the relative density to water D_r and void ratio e, as shown in Table 2.3.

In 1992, Rix and Stokoe [150] proposed a calculation of maximum shear modulus:

$$G_{max} = 1634 \cdot (q_c)^{0.250} \cdot \left(\sigma'_v\right)^{0.375} \tag{2.10}$$

where q_c is cone resistance obtained from the cone penetration test (Sect. 1.9.6), defined as the force acting on the cone divided by the projected area of the cone; σ'_v is the vertical effective stress.

Figure 2.7 shows an example of the resulting estimates of G_{max} in an upper sand layer at a North Sea site. It is obvious that the estimates based on different methods differ to some extent. Practically, the final design G_{max} can sometimes be taken as the average of the resulting estimates by all methods.

For clay, G_{max} can roughly be estimated from its correlation with penetration parameters obtained in an in situ test, which is shown in Table 2.4.

For clay, Mayne and Rix [152] presented a calculation of G_{max} based on the cone penetration correlation with a constant tip resistance of 2 MPa:

$$G_{max} = 406 \cdot (q_c)^{0.695} \cdot e^{-1.130} \tag{2.11}$$

Table 2.3 $K_{2,max}$ as a function of relative density to water D_r and void ratio e [149]

e	$K_{2,max}$	D_r (%)	$K_{2,max}$
0.4	70	30	34
0.5	60	40	40
0.6	51	45	43
0.7	44	60	52
0.8	39	75	59
0.9	34	90	70

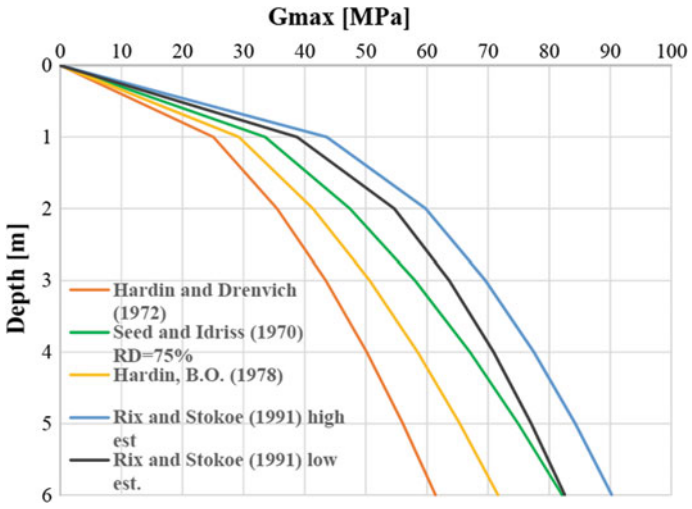

Fig. 2.7 An example of G_{max} estimated by different formulations. The upper and lower estimates based on the method proposed by Rix and Stokoe [150] correspond to upper and lower cone resistance (courtesy of Aker Solutions and NGI)

Table 2.4 G_{max}/s_u (s_u is the undrained strength measured in a consolidated–undrained triaxial shear test, see Sect. 1.9.3) [151]

I_p	*OCR*		
	1	2	5
15–20	1100	900	600
20–25	700	600	500
35–45	450	380	300

Based on various laboratory results available for different types of soils, Santos [155] proposed two unified curves representing the lower- and upper-bound values of G_{max}:

$$G_{max} = 4000e^{-1.3}p_a^{0.5} \text{ for the lower-bound} \tag{2.12}$$

$$G_{max} = 8000e^{-1.1}p_a^{0.5} \text{ for the upper-bound} \tag{2.13}$$

where e and p' are void ratio and the mean effective normal stress, respectively.

The two equations above for a given value p_a = 100 kPa (atmospheric pressure) are given in Fig. 2.8.

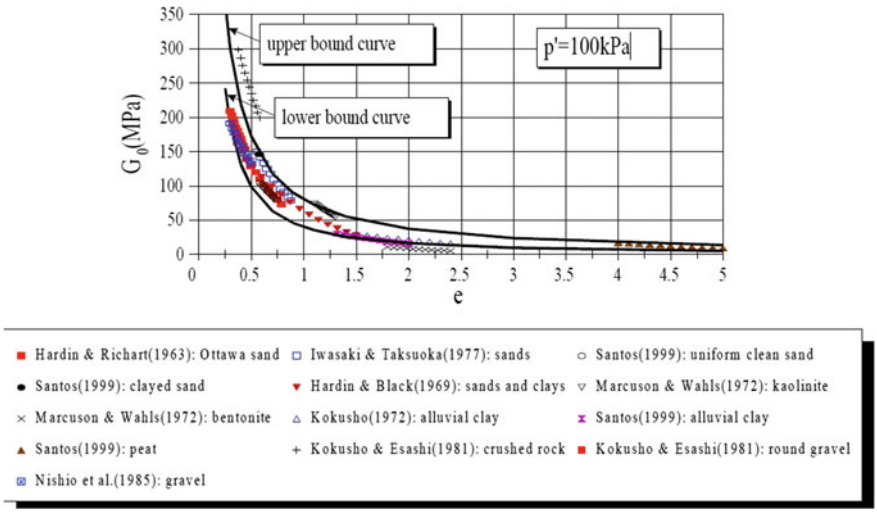

Fig. 2.8 Lower and upper bounds of $G_{\max}$ [156] ($p' = p_a = 100\,\text{kPa}$)

2.2.3 *Equivalent Damping Modeling*

Responses of soil are mainly influenced by both mechanical properties of soil and the characteristics of loading. Static loading is the simplest one and often well described. Long-duration cyclic loading may generally result in a noticeable degradation in soils' mechanical properties. Furthermore, strictly speaking, dynamic loading impedance (Sect. 5.4) is also partially determined by damping related to loading rate, even though seismic loading, being a form of short-duration, cyclic, high-rate loading, is somewhat different in this sense. Therefore, predicting actual soil responses is complicated and often poorly presented in overly simple models. Reliable simple models with which to represent soil damping are essential for performing efficient calculations of dynamic soil responses, and the equivalent damping model is widely adopted for this sake.

To describe the equivalent damping model in soil dynamics, we first go through the concept of equivalent damping in engineering dynamics [123]. Even though viscous damping modeling has obvious advantages, the energy dissipation for actual soil is both displacement proportional and velocity proportional. This leads to the concept of equivalent viscous damping, which is used to define the damping of a system using viscous damping based on the equivalent energy dissipation between the viscous damping and that of the actual system. In case of relatively low damping (less than 15%), viscous, friction, and hysteretic damping can be conveniently expressed by a unified model called equivalent viscous damping.

Consider an SDOF system with viscous or hysteretic damper (Fig. 2.9) subjected to harmonic loading $F(t) = F_0 \sin(\Omega t)$, where F_0 is the maximum amplitude of $F(t)$. It is noted that the work done by conservative forces such as elastic, inertia,

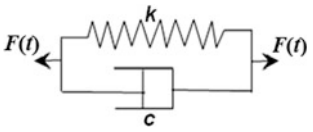

Fig. 2.9 Physical representation of frequency-dependent hysteretic damping mechanism

and gravitational forces in a complete loading cycle will be zero. Therefore, the network is dissipated by damping only. The left figure of Fig. 2.10 illustrates the energy dissipation (E_d) during a complete cycle by viscous damping when the motions reach a steady state, which can be expressed as:

$$E_\mathrm{d} = \int F_\mathrm{d}\mathrm{d}\delta = \int_0^{2\pi/\omega} (c\dot{\delta})\dot{\delta}\mathrm{d}t = c\int_0^{2\pi/\omega} [\Omega X_{0\mathrm{d}}\cos(\Omega t - \phi)]^2\mathrm{d}t = \pi\Omega c X_{0\mathrm{d}}^2 \quad (2.14)$$

From the equation above, it is found that, rather than being a constant value, the energy dissipation is proportional to the excitation frequency Ω or the square of the motion amplitude $X_{0\mathrm{d}}$.

Furthermore, the equation above is only valid with the presence of spring stiffness k, as shown in the middle figure of Fig. 2.10, which gives:

$$E_\mathrm{d} = \pi\Omega c X_{0\mathrm{d}}^2 = 2\pi\zeta\frac{\Omega}{\omega_n}kX_{0\mathrm{d}}^2 \quad (2.15)$$

With total energy expressed as either the maximum potential/strain energy ($\frac{1}{2}kX_{0\mathrm{d}}^2$) or the maximum kinetic energy ($\frac{1}{2}m\Omega^2X_{0\mathrm{d}}^2$), one can measure the dissipation as a fraction of the total energy, called specific damping capacity:

$$\frac{E_\mathrm{d}}{E_\mathrm{total}} = \frac{2\pi\zeta\frac{\Omega}{\omega_n}kX_{0\mathrm{d}}^2}{\frac{1}{2}kX_{0\mathrm{d}}^2} = 4\pi\zeta\frac{\Omega}{\omega_n} \quad (2.16)$$

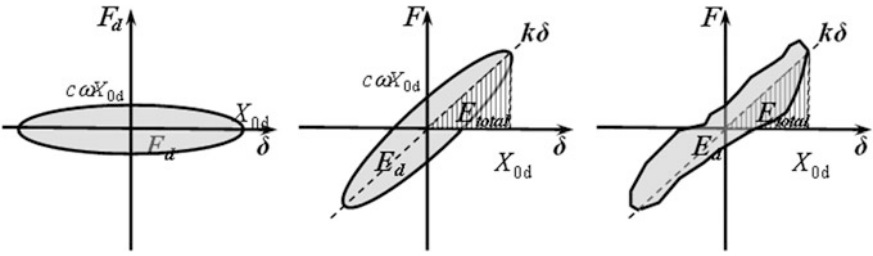

Fig. 2.10 Energy dissipation and strain energy by a viscous damper (left, strain energy is zero), hysteretic damper (middle), and real measurement (right)

If the loss of energy due to damping is only supplied by the excitations, the steady-state responses can only be reached if the excitation frequency Ω is equal to the soil system's nature frequency ω_n. Therefore, the specific damping expressed by the equation above can be rewritten as:

$$\frac{E_\mathrm{d}}{E_\mathrm{total}} = 4\pi\zeta \tag{2.17}$$

Realistic measurement of force-response diagram (right figure of Fig. 2.10) does not show a perfectly ellipse shape. However, damping level can be conveniently calculated by measuring the total energy (E_total) and energy dissipation (E_d) as shown in the right figure of Fig. 2.10.

The most convenient determination of equivalent damping ζ_eq is by measuring the harmonic force and harmonic responses at $\Omega = \omega_n$:

$$E_\mathrm{d} = E_\mathrm{total} 4\pi\zeta_\mathrm{eq} \frac{\Omega}{\omega_n} = E_\mathrm{total} 4\pi\zeta_\mathrm{eq} \tag{2.18}$$

This gives:

$$\zeta_\mathrm{eq} = \frac{E_\mathrm{d}}{4\pi E_\mathrm{total}} \tag{2.19}$$

If one replaces the force F and displacement δ by the shear stress τ and strain γ in Fig. 2.2 and replaces the stiffness k by the secant shear modulus $G_\mathrm{sec}(\gamma')$ at the maximum shear strain γ', resulting in Fig. 2.11, the equation above can be reformulated as:

$$\zeta_\mathrm{eq} = \frac{E_\mathrm{d}}{4\pi E_\mathrm{total}} = \frac{1}{2\pi} \frac{A_\mathrm{loop}}{G_\mathrm{sec}(\gamma')\gamma'^2} \tag{2.20}$$

where A_loop is the area of the hysteresis loop shown in Fig. 2.11.

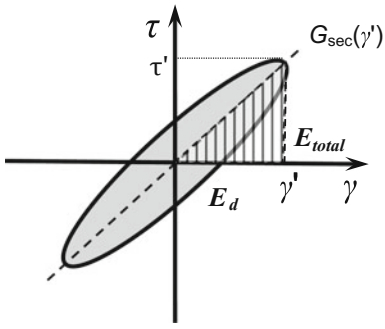

Fig. 2.11 Energy dissipated in one cycle E_d and the total energy (maximum strain energy) stored in one cycle E_total in a hysteresis loop

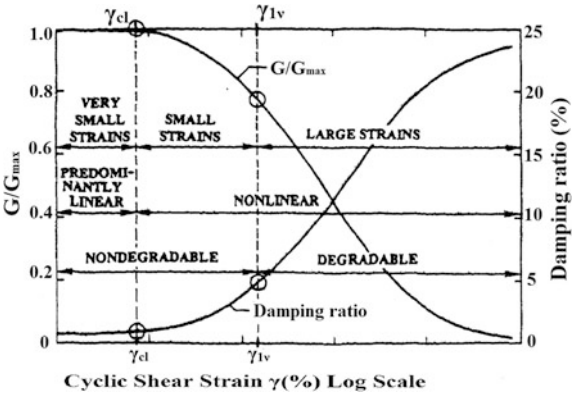

Fig. 2.12 Curves of secant modulus reduction (expressed in normalized terms) and damping (expressed in absolute terms) varied with the cyclic shear strain [118], γ_{cl} and γ_{1v} are the linear threshold shear strain and the volumetric cyclic threshold shear strain, respectively

The soil damping is mainly influenced by the cyclic strain amplitude, soil type, mean effective confining stress, plasticity index, frequency of loading, and the number of loading cycles. Soil damping generally decreases with an increase in mean effective confining stress for all strain amplitudes. Even though soil damping generally increases with an increase in plasticity index, at high strain levels, it even decreases with an increase in plasticity index [124, 125]. Moreover, as soil damping is strongly influenced by the frequency of loading and the number of cycles, it is suggested that one measure the damping value at frequencies and number of loading cycles similar to those of the anticipated cyclic and dynamic loadings.

The secant shear modulus $G_{sec}(\gamma')$ and equivalent damping ζ_{eq} are often referred to as equivalent linear material parameters as shown in Fig. 2.12, which will be further discussed in Sect. 2.3.

2.3 Soil Stiffness and Damping Modeling in an Equivalent Linear Model

2.3.1 Trends in Dynamic Soil Properties and Strain Thresholds

Based on the conceptual framework of soil behavior varied with strain [126, 127] and stress–strain response [128], several strain levels can be defined, as presented by Atkinson and Sallfors [129] and Vucetic [118] (shown in Fig. 2.12): the very small strain regime, where the stiffness modulus is constant and soils show elastic behavior; the small strain regime, where the stiffness modulus varies nonlinearly with the strain; and the large strain regime, where the soil is close to failure and the soil stiffness is relatively small. The large strain regime is sometimes further divided into medium strain regime and large strain regime.

For all types of soils, there is a strain γ_{c1} (some literatures use γ_{tl}), called linear threshold shear strain as shown in Fig. 2.12, or also called nonlinearity threshold by Vucetic and Dobry [231]. Below γ_{c1}, the shear modulus measured from tests under either drained or undrained conditions is similar because no notable excess pore pressure can be generated at such a small strain level. Above γ_{c1}, the nonlinear behavior of soil stiffness appears.

The region below γ_{c1} is called the very small strain elastic regime (some literatures also call it the small strain regime [144]) since the soil with strains at this regime essentially exhibits linear-elastic material behavior, i.e., the soil stiffness is approximately constant, bonds at molecular level remain unchanged, very minor energy is dissipated, and no pore-water pressure is generated. γ_{c1} is normally at a shear strain level of 0.0005–0.003%, corresponding to a modulus reduction G/G_{max} of around 0.98–0.99. The main source of energy dissipation is friction between soil particles and/or viscosity, and the material damping ratio is constant at a minimum value, also called the small-strain damping ratio ξ_{min}.

Just above linear threshold shear strain γ_{c1}, soils behave nonlinearly but still elastically with minor fabric change, i.e., the stress–strain relationship is curved, but the deformation is recoverable upon unloading. There is no accumulation of pore-water pressure during undrained cyclic loading and no volume change for drained conditions. The upper-bound value of this nonlinear-elastic region is called elastic threshold strain, which is typically at a shear strain level of around 0.005%. Due to the increased cyclic strain level compared to the very small elastic strain regime, the material damping is slightly increased. Obviously, elastic threshold strain establishes the difference, among strain regimes, between fully recoverable behavior and strength degradation.

Volumetric cyclic threshold shear strain or degradation threshold [231] occurs when the strain further increases to a level below which the structure of soils does not change, and beyond which the soil skeleton (microstructure) starts to change irreversibly, indicating the onset of volume change (drained condition) and possible pore-water pressure generation (undrained condition). This strain level is commonly notated as γ_{1v} or γ_{tv}, as shown in Fig. 2.12.

The region below γ_{1v} but above the linear threshold shear strain (γ_{c1}) is defined as the small strain regime, as shown in Fig. 2.12. At γ_{1v}, soil deformations become irrecoverable. γ_{1v} has been derived from strain-controlled conditions [126] and stress-controlled conditions [130, 131]. For sands, γ_{1v} is in the order of 0.01%; while for clay, this value can be one order of magnitude larger. For example, Hsu and Vucetic [132, 133] presented that, for silts and clays having plastic index from 14 to 30, γ_{1v} ranges from 0.024 to 0.06%. Such difference indicates that γ_{1v} depends on the microstructure of soils and is likely to be influenced by the soils' plasticity index. Its value relates to both G/G_{max} ratio ranging from 0.6 to 0.85 and a material damping ranging from 2 to 4% (in absolute terms) which is higher than the small-strain damping ratio ξ_{min} (Sect. 2.3.3).

There is also yet another strain value, called large strain threshold γ_{td}. γ_{td} represents the higher strain value that induces the decisive de-structuring of soil specimen. γ_{td} has been derived from stress-controlled conditions [134] and used as a

type of strain threshold by Diaz-Rodriguez [135]. The large strain threshold has been represented as a critical level of cyclic loading below which soil failure will never occur. Below this loading, soil exhibits a hysteretic equilibrium behavior and a nearly elastic pore pressure response. In some tests for clays, high residual pore pressure under the critical stress ratio can be observed, which potentially accelerates soil creep and eventual failure under undrained condition. The effects of cyclic loading associated with the strain level around γ_{td} have been investigated through experiments, in which 30,000 [136] to 300,000 cycles [137] of loading have been applied during tests. This amount of cycles is regarded as far greater than any realistically possible real-world scenario, because even for offshore structures subject to continuous ocean wave loading, undrained shearing is unlikely to persist for more than 1000 loading cycles [138]. Under such critical cyclic stress, the first cycle of loading predominantly causes deformations and the accumulation of pore-water pressure [81, 136], and a gradual stabilization or strain-hardening can be reached [139].

As shown in Fig. 2.13, the majority of geotechnical engineering issues are associated with the small strain and large strain regimes.

Reference [139] presents a review of various types of strain thresholds used in soil dynamics.

Along with strain level, effective confining pressure, plasticity characteristics, etc., also significantly influence both the modulus reduction curve and the damping. For example, at the same strain level, the shear modulus reduction is more significant for low-plasticity than for high-plasticity soils. The damping ratio is higher

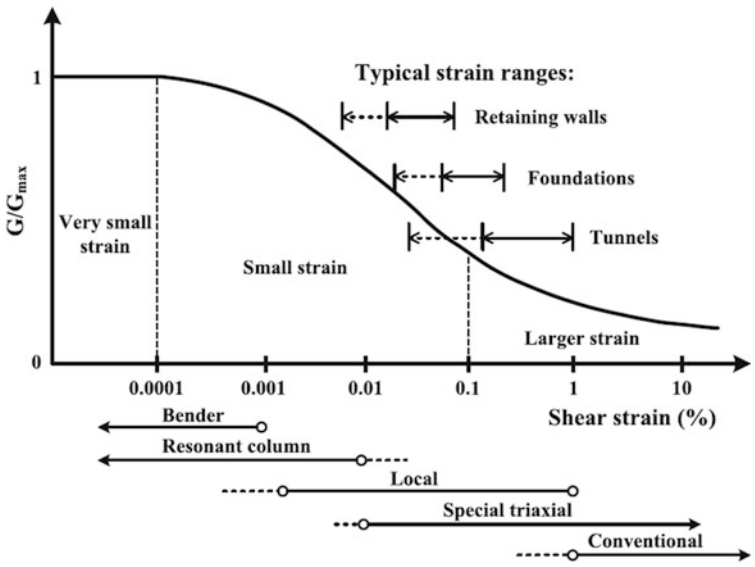

Fig. 2.13 Normalized stiffness degradation curve with corresponding geotechnical applications [140]

Table 2.5 Parameters that control nonlinear soil behavior and their relative importance in terms of affecting shear modulus and material damping presented by Hardin and Drnevich [141]

Parameters	Impact on shear modulus		Impact on material damping	
	Clean sands	Cohesive soils	Clean sands	Cohesive soils
Strain amplitude	***	***	***	***
Mean effective confining pressure	***	***	***	***
Void ratio	***	***	***	***
Number of loading cycles	+	*	***	***
Degree of saturation	*	***	**	–
OCR	*	**	*	**
Effective strength envelope	**	**	**	**
Octahedral shear stress	**	**	**	**
Frequency of loading (above 0.1 Hz)	*	*	*	**
Other time effects (thixotropy)	*	**	*	**
Grain characteristics, size, shape, gradation, mineralogy	*	*	*	*
Soil structure	*	*	*	*
Volume change due to shearing strain below 0.5%	–	*	–	*

***: Very important
**: Less important
*: Relatively unimportant
+: Relatively unimportant except for saturated sand
−: Unknown

for low-plasticity than for high-plasticity soils. Tables 2.5 and 2.6 rank the relative importance of various soil parameters on the shear modulus and material damping, as presented by Hardin and Drnevich [141] and Darendeli [144], respectively.

The current state of the practice to determine soil stiffness and damping comprises measuring and estimating (1) shear wave velocity, (2) soil stiffness varied with shear strain, (3) soil damping varied with shear strain. Furthermore, more recent proposed methods to estimate the soil stiffness and damping account for influences of a range of soil parameters in addition to just the shear strain, even though some of those methods involve excessively complex procedures and are essentially not suitable—or even feasible—for engineering practice.

Table 2.6 Parameters that control nonlinear soil behavior and their relative importance in terms of affecting normalized modulus reduction and material damping curves presented by Darendeli [144]

Parameters	Impact on normalized shear modulus reduction curve	Impact on material damping curve (Sect. 2.3.3)
Strain amplitude	***	***
Mean effective confining pressure	***	***
Soil type and plasticity	***	***
Number of loading cycles	*+	***++
Frequency of loading (above 1 Hz)	*	**
OCR	*	*
Void ratio	*	*
Degree of saturation	*	*
Grain characteristics, size, shape, gradation, mineralogy	*	*

***: Very important
**: Important
*: Less important
+: On competent soils included in the study by Darendeli [144]
++: Soil type dependent

2.3.2 *Stiffness Modeling*

2.3.2.1 General

Stiffness modeling in an equivalent linear model that requires two types of information can be obtained from either established equations or testings. The strain level and the testing apparatus used to obtain the two types of information are different. The first type is related to very small strain properties, tested with, for example, the resonant column apparatus (Chap. 6), where the major focus is on the determination of $G_{\max}$. The second type is to model the changes in shear modulus and damping ratio varied with shear strain, which are measured with various types of cyclic loading test apparatus and cover a larger strain level [139]. Sections 2.3.2 and 2.3.3 will present the modeling of soil stiffness and damping, respectively. The relevant testing methods will be presented in Chap. 6.

2.3.2.2 Modulus Reduction Curve

Extensive experimental data for modulus reduction (also called normalized shear modulus) curves $G/G_{\max}$ are accessible through various published researches. In

those studies, typically "average" normalized modulus reduction and material damping curves (Sect. 2.3.3) have been presented. There are typically two elements to establish such curves: (1) Determine the target shape of the modulus reduction curve; (2) Select model parameters that describe the target relationships with reasonable simplification/approximation. Several well-recognized hyperbolic soil models [118, 141–143] have been proposed, making the analysis possible even without running relevant laboratory tests.

Hardin and Drnevich [141] assumed that the stress–strain curve of soils can be represented by a hyperbola asymptotic to the maximum shear stress, and the normalized modulus reduction curve may be expressed as:

$$\frac{G}{G_{\max}} = \frac{1}{1 + (\gamma/\gamma_{\mathrm{r}})} \tag{2.21}$$

where G is the shear modulus at shear strain $\gamma\,(\%)$; the reference strain $\gamma_{\mathrm{r}} = \frac{\tau_{\max}}{G_{\max}}$.

Hardin and Drnevich [141] also observed that soil type has an impact on the stress–strain relationship and found through measurement that stress–strain curves deviate from the simple mathematical model depending on the soil type. Therefore, they proposed to approximate the observed soil behavior by distorting the strain scale so that the measured stress–strain curve can have a hyperbolic shape. For this purpose, they defined a hyperbolic strain γ_{h}, which replaces the $\gamma/\gamma_{\mathrm{r}}$ term in the equation above:

$$\gamma_{\mathrm{h}} = \frac{\gamma}{\gamma_{\mathrm{r}}}\left[1 + a \cdot \exp\left(-b \cdot \left(\frac{\gamma}{\gamma_{\mathrm{r}}}\right)\right)\right] \tag{2.22}$$

where a and b are coefficients that adjust the shape of the stress–strain curve for different soil types, number of cycles, and loading frequencies.

The empirical equations proposed by Hardin and Drnevich [141] account for the effects of plasticity index, over-consolidation ratio, and confining pressure mainly through adjusting reference strain γ_{r}. Effects of soil type, number of loading cycles, loading frequency, and saturation are taken into consideration by adjusting $\xi_{\max}$ (the maximum damping ratio of the soil presented in Sect. 2.3.3) and the a and b coefficients in the equation above. Although complexities of the procedure in the equation proposed by Hardin and Drnevich [141] militate against their extensive application, their work represented an important step forward in characterizing dynamic soil behavior [144].

It is noticed that in the proposed equation by Hardin and Drnevich [141] above, only one curve fitting variable (reference strain γ_r) is involved, making it difficult to fit to experimental data. To solve this problem, Stokoe et al. [143] and Darendeli [144] proposed that modulus reduction curves can be established by fitting the experimental data into the equation as follows:

$$\frac{G}{G_{\max}} = \frac{1}{1 + (\gamma/\gamma_t)^{\alpha}} \tag{2.23}$$

where α is a curvature parameter ($\alpha = 1.0$ corresponds to a standard hyperbolic backbone curve) and can normally be taken as 0.92; γ_t is called the pseudo-reference strain, corresponding to the shear strain when $G/G_{\max} = 0.5$; empirical relationships exist to predict γ_t as a function of basic parameters such as plasticity index I_p, overburden (effective confining) stress σ'_m, and over-consolidation ratio (OCR):

$$\gamma_t = \left(\varphi_1 + \varphi_2 \cdot I_p \cdot \mathrm{OCR}^{\varphi_3}\right) \times \sigma_m'^{\varphi_4} \tag{2.24}$$

where $\varphi_1 = 0.0352$; $\varphi_2 = 0.0010$; $\varphi_3 = 0.3246$; $\varphi_4 = 0.3483$.

It is noticed that, in the equation describing modulus reduction curves, pseudo-reference strain γ_t is used to avoid confusion with the reference strain as defined by Hardin and Drnevich [141]. The advantages of using the pseudo-reference strain are: (1) γ_t can be conveniently evaluated from the material-specific modulus reduction curves obtained from laboratory tests; (2) even if in many cases, material-specific testing is not available, empirical relationships do exist to predict γ_t [144, 145]. However, because pseudo-reference strains are determined from modulus reduction curves that are typically defined for strains less than 1%, a backbone curve described by a hyperbolic curve fit using γ_t may not accurately represent soil behavior at large strain level [146].

To develop the two equations above, Darendeli [144] used an extensive database from various research projects. The database consisted of combined resonant column (Chap. 6) and cyclic torsional shear (Sect. 6.3.2.2) tests, sequentially performed on intact samples from soils described as having low void ratio and not liquefiable during earthquakes. The tested soil samples ranged from natural clean sands to clays, characterized by broad intervals of sampling depth (3–263 m), confining pressure (0.3–27.2 atmosphere pressure), I_p (0–132%) and OCR (1–8). A statistical analysis of the database was undertaken to calibrate all of the required parameters.

2.3.3 Damping Modeling

Energy dissipation occurs even if the level of soil's shear strain is rather small [144]. This is still not fully understood, as theoretically, the damping exists only when soil strain is above a threshold value.

In geotechnical engineering, a typical way to specify the soil damping is to relate it to the strain level or $G/G_{\max}$. Borden et al. [157] and Ishibashi and Zhang [158] established the relationship between soil damping and $G/G_{\max}$ using a polynomial

expression. Hardin and Drnevich [141] proposed an approximate shape for the material damping curve as:

$$\frac{\xi}{\xi_{\max}} = \frac{\gamma/\gamma_r}{1+(\gamma/\gamma_r)} = 1 - \frac{G}{G_{\max}} \tag{2.25}$$

where $\xi_{\max}$ is the maximum damping ratio of the soil, which depends on soil type, confining pressure, number and frequency of cyclic loadings.

Note that, among those models, the influence from plasticity index (I_p) is not included, even if it is a rather important parameter to affect the soil damping. At the reference soil confining pressure p_a = 100 kPa, the small-strain damping ratio ($\xi_{\min}$) increases proportionally to the increase in I_p:

$$\xi_{\min(ss)} = a(I_p) + b \tag{2.26}$$

where a and b are fitting parameters and may be taken as 0.008 and 0.82, respectively.

Darendeli [144] and Stokoe et al. [159] proposed a rather simple damping equation by assuming Masing damping (Sect. 2.4.2) behavior [160, 161] and an adjusting function ($f(G/G_{\max})$) to fit the Masing damping to the experimental data, and by further adding the $\xi_{\min}$ to calculate the total damping:

$$\xi = f(G/G_{\max}) + \xi_{\min} \tag{2.27}$$

$\xi_{\min}$ in the equation above can be calculated by converting $\xi_{\min(ss)}$ at a confining pressure $\sigma\prime_m$ rather than the reference soil confining pressure p_a:

$$\xi_{\min} = \xi_{\min(ss)}\left(\sigma'_m/p_a\right)^{-0.5k} \tag{2.28}$$

where p_a = 100 kPa (reference atmospheric pressure); k is a stress correction exponent depending on I_p and geologic age [145].

Since the value of $f(G/G_{\max}) = \xi - \xi_{\min}$ is also frequency-dependent, the best-fit curve based on torsional shear test results is more preferred, as proposed by Zhang and his co-workers [145]:

$$f(G/G_{\max}) = 10.6(G/G_{\max})^2 - 31.6(G/G_{\max}) + 21.0 \tag{2.29}$$

From the equation above, it is noticed that when $G/G_{\max} = 1$, i.e., at zero or small strain condition, the total damping ξ is equal to $\xi_{\min}$. And when $G/G_{\max} = 0$, i.e., at very large strain condition, the $\xi - \xi_{\min}$ is 21%.

Sugito et al. [153] and Assimaki et al. [154] recommended that the frequency dependence of soil damping be included in a frequency domain analysis.

2.4 Nonlinear Soil Models

2.4.1 General

Soil is a complicated material that behaves nonlinearly and often shows time-dependent behavior when subjected to time-varying stresses, and under cyclic loading, it can exhibit complex behavior associated with irregular loading, densification, pore pressure generation, etc. Therefore, to better represent the behaviors, there is a need for more dedicated constitutive laws that can incorporate both the hysteretic nature of the damping and the strain dependence of shear modulus and damping ratio.

In engineering applications, a broad range of simplified and advanced soil models have been employed to perform nonlinear soil response analysis. Those nonlinear inelastic soil properties can be modeled in two ways. The first is through cyclic soil models (Sect. 2.4.2) including backbone curves together with a number of rules that govern the unloading and reloading behavior and other effects. The second is by dedicated nonlinear constitutive soil models (Sect. 2.4.4) with a yield criterion/surface to determine the onset of the yielding and plasticity, a hardening rule to describe how the yield surface changes with the progression of plastic deformation, and a flow rule to describe the progression of yielding in the plastic domain, i.e., to define plastic strain rate outside the yield surface [123]. Such nonlinear models are normally used in time-domain response analyses.

It is noted that, theoretically, soil damping should be included in the hysteretic response modeled by nonlinear soil models. In reality, however, most soil models give nearly zero damping at small strains compared with that obtained from field measurements. Therefore, viscous damping is often used to supplement hysteretic damping from nonlinear soil models in soil response analyses. At small levels of strain, linear viscous Rayleigh damping can be used to represent the damping effects, as will be presented in Sect. 2.4.3. On the other hand, an over-estimation of damping at large strain can result when the hysteretic damping is calculated using unload–reload stress–strain loops in traditional cyclic nonlinear soil models adhering to Masing's rule (Sect. 2.4.2). A modification to reduce the damping can then be performed, as will be presented in Sect. 2.4.2.

As a general rule, for sites with soft soil or subject to strong seismic motions or high amplitude of cyclic loading, especially when the soils' shear stresses approach their shear strength, the use of stiffness and damping modeling applied to equivalent linear soil models is not appropriate. The nonlinear soil models have then to be used to calculate the nonlinear responses of soils, which are suitable to model soils with large strain amplitude.

2.4.2 Cyclic Nonlinear Soil Models

To represent the variation in shear stiffness under cyclic loading, cyclic nonlinear models are used, which can follow the actual stress–strain path (without reversal loading). A very simple way to describe this is to use a backbone curve (also called skeleton curve or initial loading curve) as shown in Fig. 2.14, which is essential to describe the soil behavior subject to initial loading. The path of the curve can easily be modeled with two parameters, the initial shear modulus $G_{\max}$ at low strain condition and the shear strength $\tau_{\max}$ at high strain level:

$$\tau(\gamma) = \frac{G_{\max}\gamma}{1 + (G_{\max}/\tau_{\max})|\gamma|} \tag{2.30}$$

To be able to represent the effects of reversal loading (the load changes its direction), besides the backbone curve, a number of rules that govern the unloading and reloading behavior and other effects must be included.

Matasovic [162] proposed a modified Kondner-Zelasko (MKZ) model to describe the hyperbolic stress–strain model with two equations, corresponding to the stress–strain relationship in the loading (backbone curve) and unloading phases, respectively:

$$\tau(\gamma) = \frac{G_{\max}\gamma}{1 + \beta(\gamma/\gamma_{\mathrm{r}})^{\mathrm{s}}} \tag{2.31}$$

$$\tau(\gamma) = \frac{2G_{\max}\left(\frac{\gamma - \gamma_{\mathrm{rev}}}{2}\right)}{1 + \beta\left(\frac{\gamma - \gamma_{\mathrm{rev}}}{2\gamma_{\mathrm{r}}}\right)^{\mathrm{s}}} + \tau_{\mathrm{rev}} \tag{2.32}$$

where γ is the given shear strain; γ_{r} is the reference shear strain; β is a dimensionless factor; $G_{\max}$ is the maximum shear modulus; and s is a dimensionless exponent; γ_{rev} and τ_{rev} are the reversal strain and stress at the hyperbolic stress–strain curve.

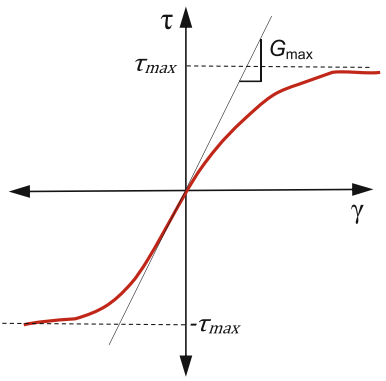

Fig. 2.14 Backbone curve showing a simple nonlinear soil model

Many nonlinear soil models to describe the hysteretic behavior for unloading and reloading follow Masing's rule [160] and extended Masing's rules [161, 163, 164], which are adopted in conjunction with the backbone curve to describe unloading, reloading, and cyclic degradation behavior of soils, as shown in Fig. 2.15. In this figure, at the initial loading stage, the stress–strain relationship follows a backbone curve as illustrated in Fig. 2.14. The shape of the stress–strain curve remains unchanged during the unloading and reloading stage, but with the origin shifted to the loading reversal point and a scaling of values of curves, which is often referred to as Masing behavior [160]. Moreover, in order to uniquely determine the stress–strain curve in irregular cycles, Kramer [1] stated that two additional rules are needed: (1) If the unloading and reloading curves cross the previous unloading and reloading cycles, the curve will follow the previous one; (2) If the unloading and reloading curves exceed the past maximum strain and intersect the backbone curve, the curve will still follow the backbone curve until the next stress reversal.

Originally developed to describe the plasticity of metal, Masing's rule assumes that both the backbone curve and cyclic response are stable. However, this may not be the case. In practice, it may be feasible to incorporate a gradual change to the backbone curve as cyclic loading effects accumulate [112]. Furthermore, the damping at large strain that results from the use of Masing's rule or the extended Masing's rule tends to be over-estimated relative to laboratory measurements [146].

On the other hand, when adopting Masing's rule and the extended Masing's rule, zero damping is implemented at small strain level, where the modulus reduction curve is linear. Even if this is theoretically true, it contradicts laboratory test observations, as at small soil strain conditions, energy dissipation does occur, as aforementioned in Sect. 2.4.1. To solve this problem, one may add a viscous damping in the form of dashpots embedded within the material elements (implemented in many codes such as DMOD_2, DEEPSOIL, OpenSees, and SUMDES) or introduce a numerical scheme that can produce nonzero damping at small strains

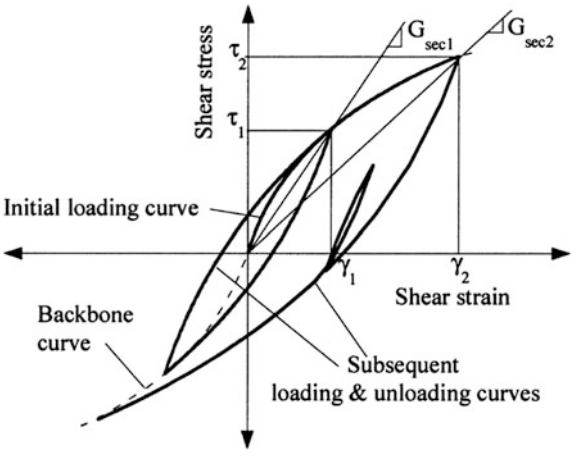

Fig. 2.15 Hyperbolic nonlinear soil model with extended Masing model to define loading and unloading behavior [165]

[164], even though the soil damping is actually neither perfectly viscous nor hysteretic [166, 167].

By introducing a reduction factor $F(\gamma_{max})$, Phillips and Hashash [168] presented a formulation that modifies the loading–unloading criteria resulting from the Masing's rules, which provides a better agreement with the damping curves for large shear strains:

$$F(\gamma_{max}) = p_1 - p_2\left(1 - \frac{G(\gamma_{max})}{G_{max}}\right)^{p_3} \tag{2.33}$$

where p_1, p_2, and p_3 are non-dimensional parameters selected to obtain the best possible fit with the target damping curve through curve fitting; $G(\gamma_{max})$ is the shear modulus at the maximum shear strain γ_{max}; G_{max} is the maximum shear modulus.

The reduction factor above can then be implemented into the backbone curve and stress–strain relationship for unloading or reloading conditions:

$$\tau(\gamma) = \frac{G_{max}\gamma}{1 + \beta(\gamma/\gamma_r)^s} \tag{2.34}$$

$$\tau(\gamma) = F(\gamma_{max}) \cdot \left[\frac{2G_{max}\left(\frac{\gamma-\gamma_{rev}}{2}\right)}{1 + \beta\left(\frac{\gamma-\gamma_{rev}}{2\gamma_r}\right)^s} - \frac{G_{max}(\gamma - \gamma_{rev})}{1 + \beta\left(\frac{\gamma_{max}}{\gamma_r}\right)^s}\right] + \frac{G_{max}(\gamma - \gamma_{rev})}{1 + \beta\left(\frac{\gamma_{max}}{\gamma_r}\right)^s} + \tau_{rev} \tag{2.35}$$

Cyclic nonlinear soil models enable the determination of shear strength and effective stress during cyclic loading, of which the latter is essential to calculate the pore-water pressure and subsequently to evaluate the potential of soil liquefaction (Sect. 7.2), given that the effective stress and the subsequent G_{max} and τ_{max} change when the pore-water pressure changes. Moreover, they are especially necessary when the shear strain level is high (above 10^{-2}) or there is permanent strain (the shear strain is not zero when the shear stress/loading is zero). All these capabilities make nonlinear soil models significantly advantageous compared to the equivalent linear soil models discussed in Sect. 2.3.

More complex cyclic nonlinear soil models are proposed by various researchers by incorporating a large number of rules to account for the effects of irregular loading, densification, pore pressure generation, etc. Due to their complexity, they are seldom used in engineering practice.

2.4.3 *Small Strain Damping Modeling in Time-Domain Analysis*

For a convenient modeling in nonlinear time-domain wave propagation analysis, rather than modeling damping by a complex hyperbolic nonlinear Masing model

(Sect. 2.4.2) or an even more complicated nonlinear constitutive soil model (Sect. 2.4.4), many time-domain site-response analysis codes include small strain damping by implementing linear viscous Rayleigh damping. This is essentially an extension of the equivalent damping model presented in Sect. 2.2.3, but with a variation of damping at different frequencies. Rayleigh damping is expressed as a linear combination of the system's mass and stiffness, as shown in Fig. 2.16, and the damping at frequency ω_i is:

$$c_i = \alpha m_i + \beta k_i \tag{2.36}$$

where α with the unit of s^{-1} and β with the unit of s are two coefficients to be determined from two given damping ratios at two specific frequencies of vibrations.

αm_i and βk_i, namely mass proportional and stiffness proportional damping, respectively, are the simplest way to formulate a proportional damping matrix, because the undamped mode shapes are orthogonal with respect to each of these [169].

α and β can be evaluated by the solution of a pair of simultaneous equations at two separate frequencies as follows:

With the orthogonality properties of mass and stiffness matrix [123], the equation above can be rewritten as:

$$2\omega_i\zeta_i = \alpha + \beta\omega_i^2 \tag{2.37}$$

Rearranging the equation above, the relationship between modal damping (ζ_i) and Rayleigh damping is finally expressed as (Fig. 2.16):

$$\zeta_i = \frac{\alpha}{2\omega_i} + \frac{\beta\omega_i}{2} \tag{2.38}$$

For soil profiles with a constant damping ratio, coefficients α and β can be computed using two significant eigenmodes i and j:

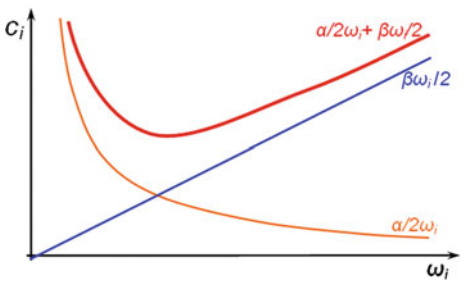

Fig. 2.16 Rayleigh damping as a function of frequency

$$\begin{Bmatrix} \zeta_i \\ \zeta_j \end{Bmatrix} = \frac{1}{4\pi} \begin{bmatrix} 1/f_i & f \\ 1/f_j & f_j \end{bmatrix} \tag{2.39}$$

And the eigenfrequency of the nth mode is calculated as:

$$f_n = (2n-1)/T_{\text{site}} \tag{2.40}$$

where T_{site} is the site period as will be presented in Sect. 3.2.

The use of a two-frequency scheme allows the model to respond to the predominant frequencies of the input motion without experiencing significant over-damping. It is normally recommended that the two specific frequencies for determining Rayleigh damping should ensure reasonable damping values in all the modes significantly contributing to the soil's dynamic response. At frequencies outside the range of these two, the damping will dramatically increase (Fig. 2.16) and the modal responses at the corresponding frequency range will almost be eliminated. Practically, this can be used to damp out the high- and low-frequency vibrations/noises that are outside the range of frequencies of interest.

The frequencies corresponding to the first-order mode of the soil column and a higher order mode that corresponds to the predominant frequency of the input motion are normally chosen to determine Rayleigh damping. Kwok et al. [170] recommended using the natural frequency and five times the natural frequency of soil columns as the two frequencies to determine Rayleigh damping. Park and Hashash [171] presented a series of recommendations for determining these two frequencies. Equal values of modal damping ratios are specified at each of the two modes. Hudson, Idriss, and Beirkae [172] suggested setting the first frequency equal to the fundamental frequency of the entire soil profile, and the second one as the closest odd number given by the ratio of the fundamental frequency of the input signal at the bedrock and the fundamental frequency of the entire soil profile. It is also suggested to keep the same value of damping, typically ranging from 0.5 to 2%, at both frequencies.

If one needs to specify damping ratios at more than two eigenmodes, instead of Rayleigh damping, an extended or more generalized form of Rayleigh damping called Caughey damping (also called the extended Rayleigh formulation) can be used:

$$c = m_n \sum_{i=0}^{N-1} \gamma_n \left(m_n^{-1} k_n\right)^n \tag{2.41}$$

where γ_n is a constant, and n is the number of modes one wants to specify damping; m_n and k_n are the modal mass and stiffness corresponding to mode n; N is the number of modes incorporated.

The modal damping ratio ζ_n at modes n can then be expressed as:

$$\zeta_n = \frac{1}{2}\sum_{n=0}^{N-1} \gamma_n \omega_n^{2n-1} \tag{2.42}$$

Note that the equation above implies that the damping can be extended to include any number of frequencies/modes. The resultant Caughey damping is then numerically ill-conditioned since $\omega_n^{-1}, \omega_n, \omega_n^3, \omega_n^5, \ldots, \omega_n^{2n-1}$ differ by orders of magnitude.

The mass and stiffness matrices adopted in formulating Caughey damping satisfy the mode shape orthogonality condition. However, Caughey damping normally results in a full matrix, which is computationally demanding for solving equations of motions.

When utilizing Caughey damping, it must be observed that using more than four frequencies/modes can result in a singular matrix depending on ω_n such that γ_n cannot be calculated. An increase in the frequencies/modes used in the calculation of the damping matrix also leads to an increase in the number of diagonal bands of the viscous damping matrix and therefore a significant time increase for solving the wave propagation problem. In addition, one must be careful in selecting the number of frequencies/modes to be employed so as not to obtain negative damping [87]. Incorporating an odd number of modes will result in negative damping at certain frequencies [169].

2.4.4 Nonlinear Constitutive Soil Models

Similar to the representation of a nonlinear material stress–strain constitutive relationship [173], a more fundamental, universal, and accurate way to describe nonlinear soil behavior is to adopt a constitutive model of soil materials using principles of material mechanics. This involves the modeling of initial stress conditions on the basis of a wide variety of stress paths, rotating principal stress axes, cyclic or monotonic loading, high or low strain rates, and drained or undrained conditions [1].

Under reversal loading, yielding due to unloading normally occurs prior to the stress reaching the yield strength, i.e., a hardening in one direction will lead to a softening in subsequent loading in the opposite direction. To account for this early yielding effect, the kinematic hardening rule with multiple yield surfaces/lines is often used as a convenient way to describe the pre-failure of soils. The rule states that the shape and size of yield surface do not change, while the center of the yield surface changes in the stress space. This is illustrated in Fig. 2.17 for a two-dimensional soil stress state.

The convenience of this approach lies in the fact that it gives a gradual change in soil stiffness, as more surfaces/lines can be used to increase the smoothness of this change. Furthermore, it can also describe the influences from the intermediate past load history. Moreover, kinematic hardening also allows a possible implementation

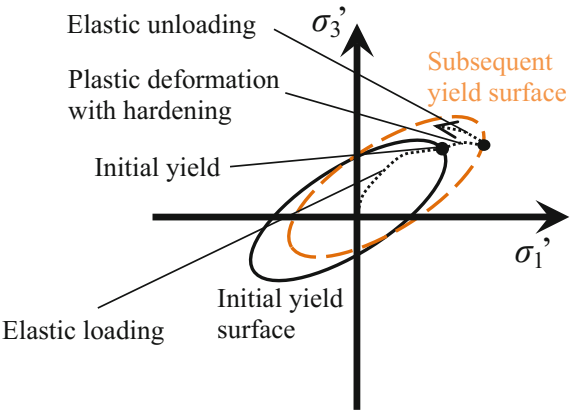

Fig. 2.17 Kinematic hardening rule in a two-dimensional principal stress space ($\sigma_1\prime$ and $\sigma_3\prime$ are the maximum and minimum principal stresses)

of anisotropic behavior of soils. In kinematic hardening, when the stress point touches the yield surface as shown in Fig. 2.17, plastic strain will then occur and can be evaluated by the flow rule. The surface is dragged by the stress point, following a kinematic hardening rule until the surface contacts the state boundary surface (SBS). Various formulations of SBS have been proposed, such as those by Dafalias and Herrmann [174], the Hashiguchi model (two- and three-surface models) proposed by Hashiguchi [175], and the MIT-E3 model proposed by Whittle [176]. The two-surface model is adopted due to its simplicity and can capture three types of soil behavior: (1) fully elastic: when the stress state is within the initial elastic yield surface; (2) transitional zone: with stress state point on the initial yield surface but inside the subsequent yield surface; (3) fully plastic: when the initial yield and subsequent yield surface come into contact, which is the normally consolidated state condition.

For engineering and research purposes, a large number of constitutive soil models have been proposed, including the Mohr-Coulomb, Drucker-Prager, Cam-Clay [177], modified Cam-Clay, modified Duncan-Chang or hyperbolic, PLAXIS soft soil (creep), PLAXIS hardening, hyperelastic, hypoelastic, viscoelastic, and viscoplastic soil models. Source [178] presents a review of soil constitutive models above. Some of those models are briefly discussed below.

The simplest soil model is to represent the soil behavior with an elastic-perfectly plastic model, which is referred to as the Mohr-Coulomb model. It is essentially a combination of Hooke's and Coulomb's laws formulated in a plasticity framework. In general stress state, the model has a linear stress–strain relationship in the elastic range, with two defining parameters from Hooke's law (Young's modulus and Poisson's ratio). There are two parameters that define the failure criteria (the friction angle and cohesion) and yet another parameter to describe the flow rule: Dilatancy angleψ, which controls an amount of plastic volumetric strain developed during plastic shearing, is assumed to be constant during plastic yielding and comes from the use of the non-associated flow rule (the plastic potential function is the same as the yield function that is used to model a realistic irreversible change in volume due

to shearing) [178]. Note that the Mohr-Coulomb model does not account for any strain-hardening or softening effects, and it can then deviate from laboratory test results significantly because of this.

The Drucker-Prager model [179] is essentially a simplification of the Mohr-Coulomb model, where the hexagonal shape of the failure cone is replaced by a simple cone. It has similar pros and cons as the Mohr-Coulomb model, even though the Mohr-Coulomb model is the most widely accepted model in the geotechnical engineering community.

The Duncan-Chang model [180], also known as the hyperbolic model, is a stress-dependent model and widely applied because its soil parameters can be easily obtained directly from standard triaxial test (Sect. 1.9.3) for both clay and sand. The stress–strain curve is a hyperbola with a high degree of accuracy. It describes three important characteristics of soils including nonlinearity, stress dependence (using a power law), and inelastic behavior for both cohesive and cohesionless soils. Even though its failure criterion is defined based on Mohr-Coulomb's two strength parameters, it is a simple yet obvious enhancement to the Mohr-Coulomb model. This model can capture soil behavior in a very tractable manner on the basis of only two stiffness parameters and has been widely used by geotechnical engineers. However, in contrast to an elasto-plastic type of model, this model cannot consistently distinguish between loading and unloading, and the model is not fit for collapse load computations in the fully plastic range. The Duncan-Chang model is therefore not popular among geotechnical researchers [181].

The modified Cam-Clay [15, 182] is an elastic-plastic strain-hardening model, where the nonlinear behavior is modeled by means of hardening plasticity. The model is based on critical-state theory [183] by combining the effective soil stress and specific volume of soil in any state, and the resulting basic assumption is a logarithmic relationship between the mean effective stress and the void ratio. This model is more suitable for describing deformation than failure, especially for normally consolidated soft soils. The model also performs very well in applications involving loading conditions associated with embankments or foundations. However, the critical state had generally been limited to saturated clays and silts. It is not applicable for modeling over-consolidated clays and granular materials due to its inability to predict observed softening and dilatancy of dense sands and the undrained response of very loose sands [184].

In the hyperelastic model, the stress is a function of the current strain rather than of the previous strain history, i.e., soil is assumed to be Cauchy elastic material. This type of formulation can be quite accurate for concrete and rock in proportional loading, but the model cannot capture inelastic behaviors of concrete and rock deformation, a shortcoming that becomes apparent when the material experiences unloading. Moreover, the hyperelastic model often requires too many material parameter inputs, thus limiting its wide application [114].

Based on a discussion of pros and cons of basic and practical soil constitutive models among Hooke's law, the Mohr-Coulomb, Drucker-Prager, modified Duncan-Chang or hyperbolic, Cam-Clay, PLAXIS soft soil (creep), and PLAXIS hardening soil model, Brinkgreve [185] discussed the applicability of each model

and selection of soil parameters from correlation with laboratory testings, which can be implemented into finite element models.

When adopting constitutive soil models, it must be observed that a good constitutive model should not only be useful to its designers, but also be user-invariant [186], i.e., different users should be able to obtain same solutions.

Compared to equivalent linear soil models and cyclic nonlinear soil models, the nonlinear constitutive soil models require inputs of more material parameters. Some of them are difficult to evaluate or exhibit large scatters in their values. For example, an advanced constitutive soil model proposed by Manzari and Dafalias [187] needs to input 16 parameters including elastic parameters, critical-state parameters, and model parameters. Even though all 16 of these parameters have physical meanings, some of them cannot be determined by conventional soil tests. Therefore, the application of advanced constitutive soil models in geotechnical engineering is still rather limited, even though it has attracted an increasing effort in research and geotechnical engineering practice.

Note the fact that high-quality input data for stress–strain relationships of soil is very limited due to the high expenses of soil testing. Therefore, there is no real engineering sense in adopting complex soil models unless the required data can be obtained conveniently or the foundation under investigation is of significant importance. Furthermore, readers should also bear in mind that no single soil constitutive model can provide a completely valid description of the complex behavior of real soils under all conditions.

2.5 Strain Rate Effects Due to Seismic Loading

For sand, strain rate has little effect on soil strength, but strength may decrease due to pore-water pressure build-up. However, similar to metal materials subject to impact loading, clay soil strength depends on strain rate. It has long been recognized that the shear strength of clay soils under seismic loading is higher than that found in static loading tests [80, 81].

It has been observed in the laboratory triaxial compression test that, for low-to-medium applied strain rates of 10^{-7}–10^{-4}/s, clay soils typically show a rough increase in undrained shear strength (Δs_u) of 5–20% per log-cycle increase in the strain rate [82, 83]:

$$\Delta s_{\mathrm{u}} = \log_{10}\left(T_{\mathrm{static}}/T_{\mathrm{dyn.}}\right) \times \Delta s_{\mathrm{u},10} \tag{2.43}$$

where T_{static} is the duration of the static testing to obtain soil shear strength; $T_{\mathrm{dyn.}}$ is the time duration for increasing variable loading from zero to the peak; $\Delta s_{\mathrm{u},10}$ is the increase in undrained shear strength (Δs_{u}) (in percent) per tenfold increase in strain rate, ranging from 5 to 20%.

By applying the relationship between Δs_{u} and strain rate variation above for clay soil subject to seismic loading, and by assuming $T_{\mathrm{static}} = 500\mathrm{s}$, $T_{\mathrm{dyn.}} = 0.3\mathrm{s}$ (in case

of seismic loading), and the shear strength increases 8% per tenfold increase in strain rate, the equation above gives a 26% increase in undrained shear strength.

Therefore, most clay soils subjected to typical undrained seismic loading may exhibit an increase in shear strength by 20–50% compared with the shear strength obtained from static loading tests. The critical-state strength of clays, however, remains largely unaffected by the rate of induced strains under low-to-medium strain rates. Here, the critical-state concept states that soils and other granular materials, if continuously distorted (sheared) until they flow as a frictional fluid, will come into a well-defined critical state. At the onset of the critical state, shear distortions occur without any further changes in mean effective stress or deviatoric stress or void ratio. Readers may read [183] for further details.

OCR (Sect. 1.11.4) plays an important role in the rate-dependent mechanical response of clay. For a constant *OCR*, the deviatoric stress attains its peak at approximately the same strain level for different strain rates. However, the strain at which the peak occurs increases with increasing *OCR*. Significant post-peak softening is observed for low *OCR* of 1 and 2 due to the generation of positive excess pore pressure, while for *OCR* of 4 or greater, the post-peak softening is relatively small [84].

Moreover, it is worth mentioning that soil's shear modulus generally degrades with a decrease in strain rate, as has been presented by several researchers [85, 86] through laboratory tests. Matesic and Vucetic [86] presented that the initial shear modulus increases at a rate of about 10% per log-cycle increase in the applied strain rate. However, soil damping does not have a clear correlation with a variation in strain rate [87].

By calculating the site response by developing a series of modified equivalent linear analyses (Sect. 3.5.2) to characterize the effects of the rate-dependent soil behavior, Park and Hashash [88] concluded that, compared with the response excluding strain rate dependence, the inclusion of strain rate dependence results in up to 20% difference in the computed response for very mild ground motions, and within 10% for higher amplitude motions.

2.6 Differences Between Soil Properties Subjected to Earthquake Loadings and Ocean Wave Loadings

Even if soil properties under earthquake loading and ocean wave loading can be obtained from the same laboratory test, they can be significantly different from each other. These differences are mainly caused by the difference in cyclic loadings' type, duration, and frequency, as well as the level of cyclic shear strain.

During an earthquake event, the seismic wave travels from the earthquake source to the ground surface. Not only the zone close to the foundation but the entire soil–foundation system is influenced by the seismic wave propagation. In addition, the soil zone near the foundation is also influenced by inertia loading due to vibrations

of the structure and the foundation. On the other hand, under ocean wave loading, essentially only the soil zones close to the foundation will be influenced by the ocean wave loading and inertia loading transmitted from the structure. Therefore, under seismic loading, the shear modulus for soils far from the foundation is generally lower than that under ocean wave loading, as the shear modulus decreases with an increase in cyclic shear strain level.

As aforementioned, the level of cyclic shear strain caused by seismic loading and ocean wave loading can be significantly different. The shear modulus of the surrounding soil may be quite different as it is shear strain dependent, leading to a difference in foundation stiffness. For example, it has been reported that the calculated soil spring stiffness for a typical GBS structure in the North Sea under seismic loading is, in terms of lateral stiffness, 1.2–3.2 times that under the influence of storm wave loading, and this ratio increases to 1.3–4.0 times in terms of rocking stiffness [67]. Obviously, this is because the seismic loading is less significant than the storm loading in terms of inducing the soil's cyclic shear strain in a typical North Sea site. The opposite trend can also be found at sites with high seismicity but mild design sea state condition.

Typical ocean wave loadings have much longer durations than seismic loadings. The number of significant cycles may be 100 times higher in a storm than in an earthquake, which also contributes to the difference in soil stiffness with regard to cyclic loading.

While the dominant frequency of seismic loading is between 0.2 and 0.5 s (Fig. 9.31), the period of ocean wave loading rises to 20 s for an extreme storm and 4–7 s for a mild sea state condition. This also indicates the importance of inertia loading under seismic loading. Furthermore, the strain rate induced by seismic wave transmission is significantly higher than that induced by ocean wave loading or wave-induced foundation loading, in which the higher strain rate may affect both the strength and shear modulus of soils, as has been presented in Sect. 2.5.

http://www.springer.com/978-3-319-40357-1

Soil Dynamics and Foundation Modeling
Offshore and Earthquake Engineering
Jia, J.
2018, XXIII, 740 p. 412 illus., 258 illus. in color.,
Hardcover
ISBN: 978-3-319-40357-1